Electronic Structures of the CdSe/CdS Core−Shell Nanorods

Ying Luo[†] and Lin-Wang Wang[‡,*]

[†]Department of Physics, Beijing Normal University, Beijing 100875, China, and [‡]Computational Research Division, Lawrence Berkeley National Laboratory, Berkeley, California 94720

ARTICLE

ABSTRACT The electronic structures of the CdSe/CdS core−shell nanorods are systemically investigated by large-scale first-principles quality calculations. The effects of band alignment, quantum confinement, piezoelectric field, and dipole moments are analyzed and delineated by comparing the results of systems with or without some of these attributes. We found complicated interplays between these effects in determining the nanorod band gap and electron hole wave function localizations. The hole wave function is found to be localized inside the CdSe core, while the electron wave function is localized in the CdS shell, with its distance to the CdSe core depending on the surface passivation. The permanent dipole moment induced by different surface passivations can change the electron hole separation, while the piezoelectric effect plays a relatively minor role. Finally, we demonstrate that it is straightforward to manipulate the nanorod electronic structure by changing its CdSe core position.

KEYWORDS: nanostructure · nanorod · *ab initio* calculations · core/shell · quantum confinement

Semiconductor nanorods have attracted great attention in fundamental research as they represent new systems for which their electronic structures can be manipulated by changing the shape and composition of the system. In applications, they provide new ways for light harvesting, carrier collection, and surface catalysis.[1−3] Among semiconductor colloidal nanostructures, CdSe and CdS quantum dots and rods are excellent systems for optical and electronic applications due to their easy synthesis, super optical quality, and relatively stable surface passivation. The band gaps of CdSe and CdS are in the visible light range and can be tuned by changing the nanostructure size. This makes them good candidates for optical related applications, including solar cells and photoelectrochemical (PEC) cells. While in the early days the focus was in quantum dots, rods, and wires with one pure material, recently, the study has been shifted to heterostructure nanosystems, such as core/shell structure, nanojunctions, and nanocontacts. One reason for this change is due to the difficulty of doping small nanosystems in the size range of a few nanometers. As a result, it is difficult to form conventional p−n junctions for device applications. Even if such p−n junctions can be formed, due to the small size of the system, hence the small number of dopant atoms, the junction can have a big device-to-device fluctuation. Fortunately, the heterostructure can play the role of p−n junction in nanosystems. The different band alignment can drive the electron and hole into different locations and dissociate the excitons, which are the main functions of p−n junctions. Experimentally, such heterostructures can be synthesized with ever better control and quality. Thus, to study the role of such heterostructures and to understand how they can be used to manipulate the electron states inside the nanosystem is of paramount importance. In many previous studies, the heterostructure is in a symmetric form, that is, mostly as spherical core/shell quantum dot or cylindrical core/shell nanowire, but the most intriguing case is in the nonsymmetric nanoheterosystems, where there is more room for electronic structure manipulations. Talapin *et al.*[3] first reported the CdSe/CdS core/rod structure and linearly polarized photoemission. More recently, Luigi *et al.*[4] and Talapin *et al.*[5] have developed a better controlled seeded-growth approach to synthesize asymmetric core/shell CdSe/CdS nanorods. The samples have high photoluminescence quantum yield,[3] indicating high sample quality. Ever since the original work, there are now many other seeded-growth heterostructure nanosystems.[6,7] Metallic particles can also be grown on the surfaces of such core/shell nanorods, with the potential to extract the carriers for various types of applications.[8]

*Address correspondence to lwwang@lbl.gov.

Received for review August 17, 2009 and accepted December 15, 2009.

Published online December 31, 2009.
10.1021/nn9010279

Figure 1. CdSe/CdS core/shell nanorod.

The CdSe/CdS core/shell nanorods are intensely studied for their optical and electronic properties.[9−12] A still unsettled issue is the electron localization in the system: whether the electron is localized in the CdSe core or outside the CdSe core. While early studies showed that the electron might be outside the CdSe core,[13,14] later experiment indicated that the electron and hole might both localize in the CdSe core.[3,10] The reason for the localization can also be complicated. Besides the band alignment, there might be effects of quantum confinement, the dipole moment, and the internal electric field due to piezoelectric effects.[12] Theoretically, besides the old tight-binding calculations,[13] most calculations are done with simple effective mass theory with assumed band offsets. Thus, there is a need for more accurate *ab initio* calculations for this particular system, and there is also a need for understanding the carrier localization due to different effects.

In this paper, we use *ab initio* methods to calculate the CdSe/CdS core/shell nanorods containing thousands of atoms. We will use the charge patching method to calculate such large systems. Besides the electronic structure of this particular system, our focus will be on the reasons for the carrier localization. In particular, we will analyze the effects of band alignment, quantum confinement, piezoelectric field, and total dipole moment by comparing the results of different systems. We found that the electron wave functions are localized outside the CdSe core, but nevertheless, it can be very close to the core depending on the surface passivation, hence the total dipole moment of the system. We also found that the piezoelectric effect plays a relatively minor role in determining the wave function localization and the band gap.

The CdSe/CdS core/shell nanorod and the CdS nanorod are constructed as a wurtzite structure. The nanorod diameter is 4.30 nm, and the length is 15.48 nm with 3063 atoms (including the surface passivation pseudo-hydrogen atoms; see below) for both systems. In the core/shell nanorod, the core is a spherical CdSe with a diameter of 3.44 nm at the right-hand side of the nanorod, and it is surrounded by CdS (see Figure 1). The *c*-axis S−Cd bond in the wurtzite structure points from left (S) to right (Cd).[3,5,15]

To have a theoretical ideal passivation, we have used pseudo-hydrogen atoms (with fractional nuclei charges and numbers of electrons) on the surface of this structure,[16] which have been demonstrated to be a very efficient way to remove the surface states from the band gap energy regime.[16]

RESULTS AND DISCUSSION

Strain Profile. The atomic positions are relaxed using the valence force field (VFF) model,[17] and the hydrostatic strains of the atoms are shown in Figure 2 for one CdSe/CdS core/shell nanorod. Figure 2 shows that there is a compressive strain in the core CdSe region and a tensile strain in the shell CdS region near the core. Meanwhile, there is no strain in the CdS shell far from the core.

Effects of the Band Alignment. Before we study the electronic structure of nanosystems, we have calculated

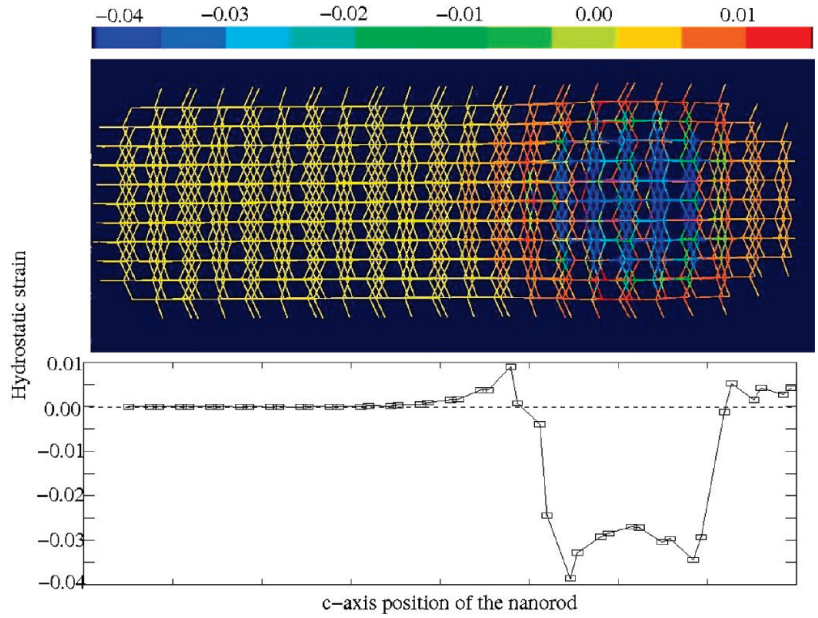

Figure 2. Hydrostatic strain in the core/shell CdSe/CdS nanorod. The lower panel depicts the strain along the central *c*-axis of the nanorod.

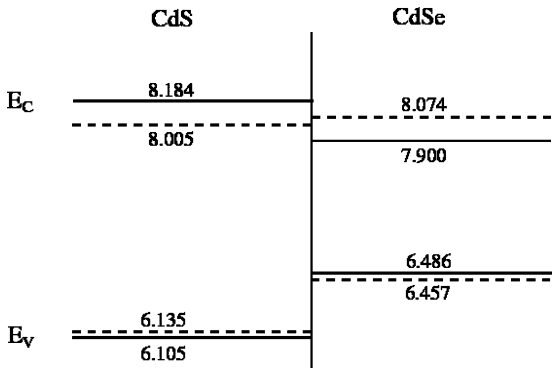

Figure 3. Band alignment of CdS and CdSe. The solid lines are the band edge energies (in eV) for natural lattice constants, and the dashed lines are the results with an average lattice constant. The spin−orbit coupling is included in this band alignment picture.

the band alignments for the bulk CdS/CdSe system. The bulk alignment can be obtained from a superlattice system with one side as CdS and one side as CdSe. We have used the zinc blende (ZB) structure and an average lattice constant of CdS and CdSe for the superlattice. The ZB band alignment should be very close to the wurtzite band alignment. The superlattice potential can be compared and aligned with the pure bulk potential with the same lattice constant. This will give us the band edge energies (deduced from the bulk band edge state calculations). The resulting band alignment is shown in Figure 3 as the dashed lines. The so-called nature band alignments (with both CdS and CdSe at their respective natural lattice constants) are obtained from the dashed lines by adding the deformation potential effects on the CBM (conduction band minimum) and VBM (valence band maximum) states. In Figure 3, the spin−orbit coupling is included for the valence band.

Note that the local density approximation plus correction (LDA+C) calculated ZB band gaps for CdS and CdSe are 2.079 and 1.414 eV, respectively. The LDA+C wurtzite band gaps for CdS and CdSe are 1.945 and 1.283 eV, respectively. These are much smaller than the experimental band gaps of 2.50[18] and 1.76 eV.[19] The reason for not correcting the local density approximation (LDA) band gaps all the way to the experimental band gaps is to get the correct effective masses,[20] which are important for describing the quantum confinement effect. However, these remaining band gap errors will not affect the relative band alignment between CdS and CdSe, for both the conduction band and the valence band. The band gap difference between the CdS and CdSe is 0.66 eV in LDA+C and 0.74 eV using the experimental band gaps. However, to get the absolute band gap for the nanostructures, it is necessary to add 0.536 eV to the LDA+C calculated result (to shift up the CBM energy).

One important feature for the band alignment is the strong effect of the strain. In the natural lattice constant, the heterostructure has a type-I band alignment with both electron and hole localized within CdSe. However, after the strain, at the average lattice constants for both CdS and CdSe (dashed line in Figure 3), the alignment for the conduction band has been changed. Now, the electron will localize weakly in the CdS. This is for the case of average lattice constant. For the actual core/shell nanorod, the magnitude of the strain might be different. We thus need direct calculations to find out where the electron will localize. We have to caution that the conduction band offset after the strain is very small. The relative size ratio between the core and the shell can change the strain profile, thus it can also change the band offset under the strain. For the actual nanorods, the other factors, such as size of the rod, size of the core, and surface passivations, can also change the localization. All of these sensitivities might have contributed to the varying experimental results.

Our calculations rely on the accuracy of the LDA band alignment for the valence band. Experience in other semiconductor heterostructures indicates that the LDA valence band alignment for similar materials (*e.g.*, with both p state top of valence band) should be reliable within about 0.1−0.2 eV. Unfortunately, at the moment, there is no other theoretical method that can yield much better results than the 0.1−0.2 eV accuracy. The GW calculation has similar accuracy. The experimental band offset also has similar accuracy. We do note that, with this accuracy, the conduction band offset in Figure 3 can change sign, as it might be caused by many other factors discussed above.

We have calculated the electronic structures for the pure CdS nanorod without CdSe core and for CdSe/CdS core/shell nanorod, both shown in Figure 4. We have first chosen Cd atom terminated surface passivation, which means there are only Cd atoms (no S atoms) on the surface of the nanorod before the pseudo-hydrogen atoms are added.[20] The pseudo-hydrogen atoms with nuclei charge $Z = 1.5$ are placed at the centers of the cutoff bonds to remove the dangling bond states.[20] The Cd-terminated surface is used in order for the nanorod to have minimum total dipole moment.

The calculated band gaps of the pure CdS nanorod and core/shell nanorod are 3.117 and 2.385 eV, respectively (already added the 0.536 eV correction for the LDA+C bulk band gap error). Thus, there is a strong quantum confinement effect, increasing the band gap by about 0.6 eV from its bulk values.

Figure 4 shows the charge densities of the conduction band minimum (CBM) and valence band maximum (VBM) states in the nanorods. For the pure CdS nanorod, there might already have been some small dipole moments. This makes the electron locate slightly at the left side, with the hole at the right side, but this dipole moment is very small. When a smaller isosurface value is used, the isosurfaces for both electron and

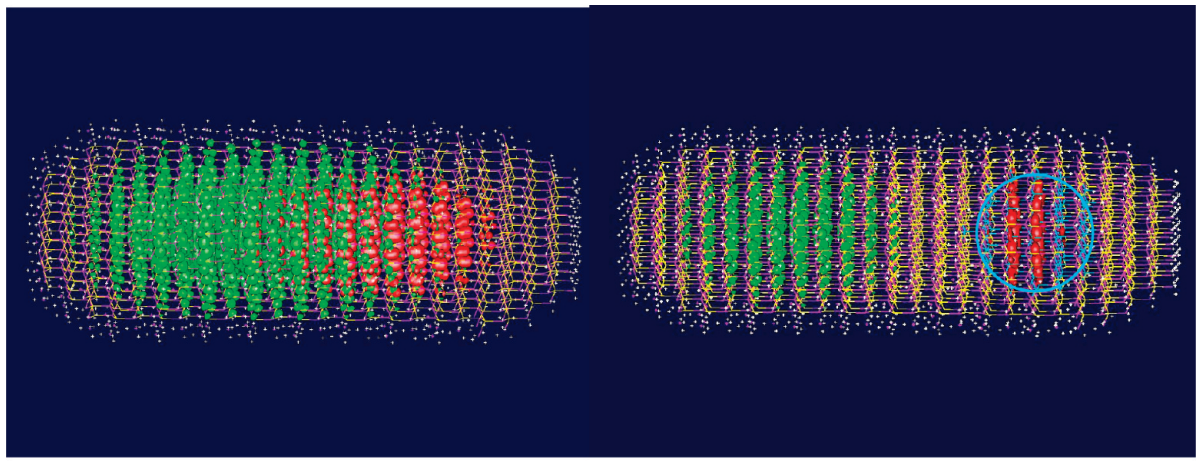

(a) (b)

Figure 4. Charge density of CBM (green) and VBM (red) states for (a) pure CdS nanorod and (b) core/shell CdSe/CdS nanorod. Both rods have Cd termination passivation. The small white dots at the surface denote the pseudo-hydrogen atoms.

hole spread out to the whole nanorod. However, when the CdSe core is added, the hole becomes completely localized inside the CdSe core. This is consistent with the valence band alignment shown in Figure 3. However, the electron is further pushed into the left CdS region. This might indicate that the CdSe conduction band edge is higher than the CdS edge, thus the strain situation is the same as shown in Figure 3. We have thus a type-II band alignment and an electron−hole spatial separation. Such separation can be very useful in some applications. For example, in a solar cell, such separation can be used to collect the electron and hole from different ends of the nanorod. Due to the large effective mass of the hole, the hole wave function is strongly localized inside the CdSe core. The localization of the hole is much more dramatic than the electron.

In a recent paper,[21] Sitt *et al.* calculated the exciton energies of the CdSe/CdS core/shell system using effective mass theory. They have used a natural conduction band offset as shown by the solid line in Figure 3, but as we show here, the strain can change the type-I band offset into a type-II band offset. In their exciton energy calculation, however, they have used a zero-order perturbation theory (using the single particle wave functions from independent electron and hole calculations to calculate the Coulomb and exchange energies). In our type-II band offset case, it is essential for a self-consistent calculation under electron−hole Coulomb interactions to determine the single particle wave functions. Due to the electron−hole Coulomb interaction, the electron wave function will likely be localized surrounding the hole, which is localized inside the CdSe core. Thus, the end result might be similar to that obtained in ref 21.

Piezoelectric Effect. It will be interesting to check the role of piezoelectric effect in the system, especially whether it will change the localization of the electron. In order to calculate the piezoelectric effect, we first calculate the stress tensor T as

$$T_j = C_{ij}\varepsilon_j \quad (1)$$

here C_{ij} is the elastic modulus. The strain tensor ε_j is obtained from our VFF calculation. We then calculate the polarization P_j through the piezoelectric formula

$$P_j = d_{ij}T_i \quad (2)$$

here d_{ij} is the piezoelectric tensor relating the polarization P_j to the stress tesnor T_i. For the hexagonal structures of CdSe and CdS, the nonzero coefficients of C_{ij} and d_{ij} are shown in Table 1.

The piezoelectric effect induced charge density ρ_{piezo} can be calculated as

$$\nabla\cdot P_{piezo} = \rho_{piezo} \quad (3)$$

and the piezoelectric potential caused by the piezoelectric charge density can be obtained by solving the following Poisson equation:

$$\nabla[\varepsilon(r)\cdot\nabla V(r)_{piezo}] = 4\pi\rho_{piezo} \quad (4)$$

here $\varepsilon(r)$ is a material-dependent dielectric constants in the nanorod. In order to see the maximum

TABLE 1. Nonzero Material Parameters of CdSe and CdS Used in the Calculations[a]

parameter	CdSe	CdS	unit
$C_{13}=C_{23}$	3.93	5.10	10^{10} N/m^2
C_{12}	4.52	5.81	10^{10} N/m^2
$C_{11}=C_{22}$	7.41	9.07	10^{10} N/m^2
C_{33}	8.36	9.38	10^{10} N/m^2
$C_{44}=C_{55}$	1.317	1.504	10^{10} N/m^2
d_{33}	10.32	7.84	10^{-2} C/N
$d_{31}=d_{32}$	−5.18	−3.92	10^{-2} C/N
$d_{15}=d_{24}$	−13.98	−10.51	10^{-2} C/N

[a]The *c*-axis of the wurtzite structure is in the 3rd direction. The parameters are taken from ref 22.

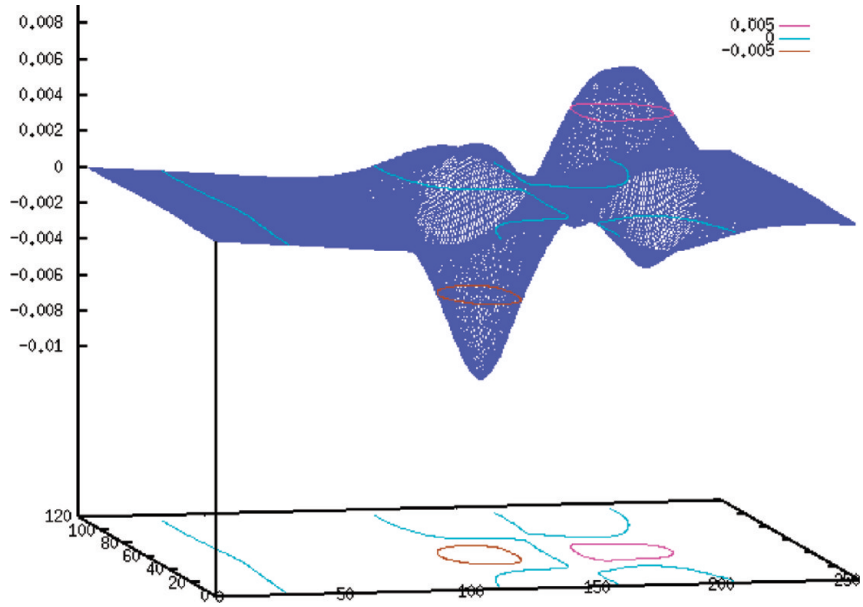

Figure 5. Potential of piezoelectric effect $V(r)_{piezo}$ on a cross section containing the *c*-axis of the nanorod. The purple, blue, and brown lines are contour lines with potential values of 0.005, 0, and −0.005 hartree. Vertical axis is the potential with the unit of hartree. The maximum potential is about 0.007 hartree at the right side interface of the core, while the minimum potential is about −0.009 hartree at the left side interface of the core. The maximum electric field (the biggest slope of the potential at $x = 150$) is at the center of the core. Shown here is the potential multiplied by the electron point charge *e*: $eV(r)_{piezo}$. Thus, it is the potential the electron will feel.

possible piezoelectric effect, we have used $\varepsilon(r) = 1$. The calculated piezoelectric potential $V(r)_{piezo}$ in the core/shell CdSe/CdS nanorod is shown in Figure 5.

The piezoelectric potential maximum and minimum are at the right and left interfaces of the CdSe core. Thus, inside the core, there is a maximum electric field that tends to push the hole toward the right-hand side, but the potential average inside the core is close to zero. To specifically test the effects of the piezoelectric potential, we substracted the piezoelectric potential, we subtracted the piezoelectric potential from charge patching method generated total potential (used for Figure 4) and then calculated the electron and whole wave functions and band gap. The modified band gap of the core/shell CdSe/CdS nanorod is 2.375 eV, which is 10 meV smaller than the original band gap. The modified wave functions are shown in Figure 6. We can see that the CBM wave function change is rather small. This is because the CBM is localized in the CdS region where the piezoelectric potential is rather small. For the hole wave function, it is still localized inside the CdSe core, but it has been pushed toward the interface due to the large piezoelectric field. From Figure 5, we can calculate the maximum electric field within the CdSe/CdS core as (0.007 + 0.009) hartree/3.44 nm = 0.127 V/nm. This is similar to the piezoelectric field in the CdSe/CdS superlattice.[22,23] Overall, we found that the effect of piezoelectric potential is small. Mind that we have artificially set the dielectric constant equal to 1, thus already significantly amplifying the piezoelectric effect. So, the real piezoelectric effect will be even smaller.

Effects of the Dipole Moments. We see from Figure 4 that there might be a small dipole moment of the nanorod in the Cd-terminated case, which causes the electron and hole to localize at different places in the pure CdS rod. There are two possible contributions to the dipole moment: one is from the bulk (due to the wurtzite structure), another is from the surface (due to surface passivation). For the Cd-terminated surface case, the surface dipole moment contribution should be minimum because there are equal numbers of surface Cd−H (pseudo-hydrogen) bonds pointing to the four possible tetrahedral bonding directions. Thus, their contributions cancel out. To test more about the effect of the dipole moment and the effect of surface passivation, we carried out the same calculations with Cd+S termination. In this termination, there are both (roughly equal number of) Cd and S surface atoms. They are passivated by $Z = 1.5$ and $Z = 0.5$ pseudo-hydrogen atoms, respectively. We also calculated a nanorod without a CdSe core and a nanorod with a CdSe core. The

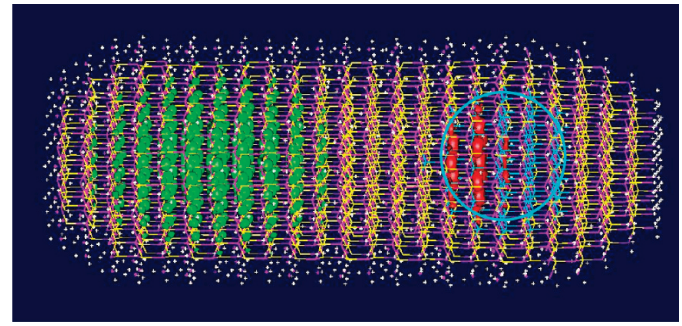

Figure 6. Modified charge density of CBM and VBM in the core/shell CdSe/CdS nanorod after the piezoelectric field has been removed.

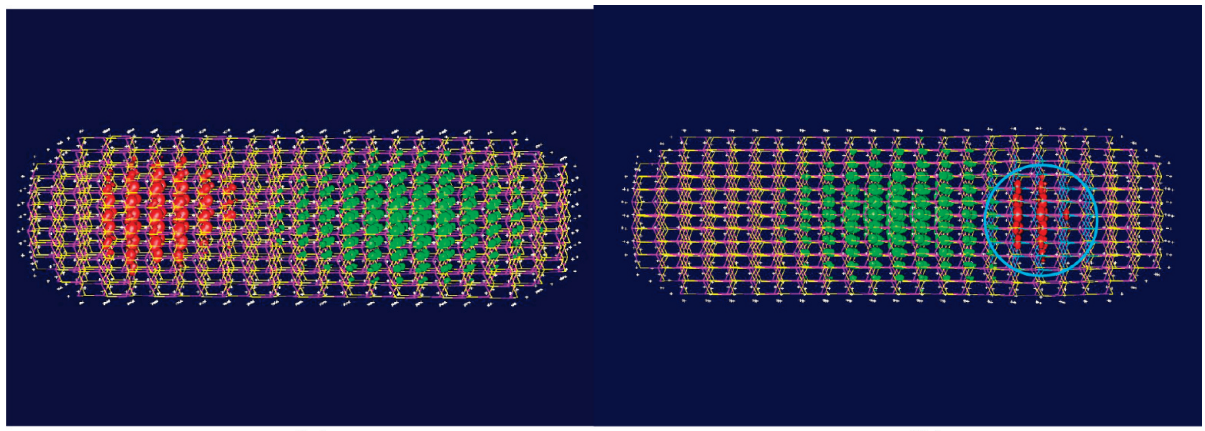

Figure 7. Charge density of the nanorods, VBM (red) and CBM (green). (a) Pure CdS rod, and (b) CdSe/CdS core/shell rod. Both rods have Cd+S surface termination.

wave function results are shown in Figure 7, and their band gaps are listed in Table 2 together with the results of the above calculated systems.

From Figure 7a, we see that the Cd+S termination reverses the dipole moment of the Cd termination result. Furthermore, the electron and hole localization in the pure CdS rod case is much stronger than the Cd termination case, indicating a much larger dipole moment coming from the surface. For the CdSe/CdS core/shell case, the electron is still localized outside the CdSe core, despite the fact the dipole moment tends to pull the electron toward the right-hand side of the rod. Compared to the Cd-terminated case shown in Figure 4, the electron is much closer to the CdSe core. Compared to the Cd-terminated results, the biggest difference is the band gap, which is increased by 260 meV. This is not caused by the piezoelectric potential. Because, according to Figure 5, when the electron is closer to the CdSe core, the piezoelectric potential will only lower the electron energy, thus reduce the band gap. In the actual calculation, removing the piezoelectric potential only changes the band gap by 16 meV. The increase of the band gap is most likely due to the decrease of the diameter of the rod. There are 3063 atoms (including the surface pseudo-hydrogen atoms) in the Cd-terminated nanorod, while there are only 2298 atoms in the Cd+S-terminated nanorod. The Cd+S termination is obtained by removing the surface Cd atoms, which have only one bond connecting to the rest of the nanorod. The smaller diameter of the rod will lead to larger quantum confinement effect, thus an increase in the band gap.

One remaining question is that why the same diameter reduction did not increase the band gap of the pure CdS and Cd+S-terminated rods from the pure CdS and Cd-terminated rods. It actually decreases the band gap by 7 meV, as shown in Table. 2. Here, the reason is more complicated. There are two factors that affect the band gap of the Cd+S-terminated rod: one is the strong dipole moment, another is the reduction of the diameter (quantum confinement effect). The former reduces the band gap by localizing the electron at the low potential side (right-hand side) and the hole at the high potential side (left-hand side), while the latter increases the band gap. Thus, the overall 7 meV reduction of the band gap is due to the winning of the dipole moment effect. This dipole moment effect is reversed, however, in the CdSe/CdS core/shell case. In this case, the electron and hole have been pushed to the opposite sides (compared to the pure CdS rod) due to be band alignment effect, thus the dipole moment might actually contribute to the increase (not decrease) of the band gap. Thus, the dipole moment effect and the quantum confinement effect work together to increase the band gap in the core/shell case.

We have only studied one geometry of the nanorod. One question is how does the role of the dipole moment change in the Cd+S-terminated nanorod when the rod length increases. First, the dipole moment comes mostly from the side surface, instead of the two end surfaces. Thus, as a result, when the rod length increases, the total dipole moment will increase proportionally. For a long rod, in a 1D picture, this is equivalent to having two fixed value (depending only on the diameter) positive and negative charges at the

TABLE 2. Band Gaps of CdS Nanorods and the Core/Shell CdSe/CdS Nanorods with Different Surface Passivations and with or without Piezo Effect[a]

rod model	piezo effect	surface passivation	band gap
pure CdS rods	no piezo effect	Cd+S	3.110 eV
		Cd	3.117 eV
core/shell CdSe/CdS rods	with piezo effect	Cd+S	2.645 eV
		Cd	2.385 eV
	without piezo effect	Cd+S	2.629 eV
		Cd	2.375 eV

[a]No piezo effect means the piezoelectric effect does not exist in those cases. The bulk band gap corrections to the LDA+C results and the spin−orbit coupling effects are already included.

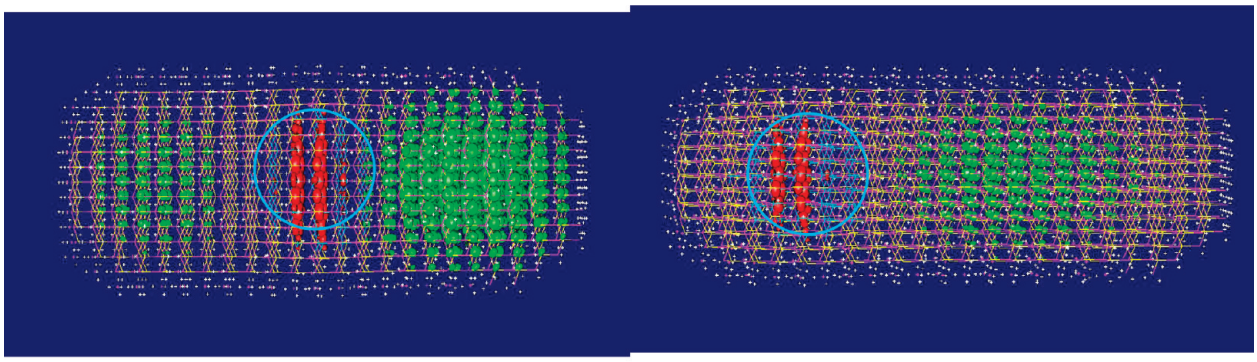

Figure 8. Electron (green) and hole (red) wave functions when the CdSe core moves from the right-hand side to the left-hand side. (a) CdSe core in the center of the nanorod, and (b) CdSe core in the right side of the nanorod. The nanorod is terminated by Cd atoms.

two ends of the rod. Thus, for a very long rod (wire), the electric field at the center of the rod will decrease, eventually going to zero, but the potential difference between the two ends will increase and saturate to a fixed value (depending only on the diameter of the rod). Thus, for Figure 7a, in a single particle picture, the electron will be located at the right-hand side, while the hole will be localized at the left-hand side. However, if a CdSe core is located at the center of the rod, then the hole will be localized inside CdSe core, and if an exciton is formed, due to electron−hole Coulomb interaction, the electron will also be localized near the center of the rod, and the dipole moment will have a very small effect on the behavior of that exciton.

Shift of the Core. Finally, we demonstrate that it is possible to control the position of the hole by shifting the position of the CdSe core. This is shown in Figure 8. Wherever the core is, the holes are always in the core and the electrons are in the shell. Thus, if it is possible to control the CdSe core position in the synthesis, it is also possible to control and manipulate the electronic structure. This can be used to design different applications based on such core/shell heterostructures.

CONCLUSION

We have systemically studied the electronic structures of the core/shell CdSe/CdS nanorod by *ab initio* quality charge patching method calculations. We have analyzed the effects of band alignment, quantum confinement, the piezoelectric field, and dipole moments. Their individual effects have been separated by comparing the calculated results for systems with and without some of these attributes.

Our calculation shows that the band alignments and the quantum confinement make the main contributions to the electron structures of the core/shell CdSe/CdS nanorod when Cd termination is used. This system has a type-II band alignment, which leads to an electron−hole spatial separation. The hole is localized in the core region, and the electron is located at the shell region. The hydrostatic strain and the deformation potential make the type-II band alignment possible. On the other hand, the effect of the piezoelectric field is small, and it only changes the band gap by less than 10 meV and slightly modifies the hole wave function position. When the system is passivated by Cd+S surface termination, there is a strong dipole moment. This dipole moment can significantly change the position of the electron wave function, making it closer to the CdSe core in the core/shell nanorod. In terms of the band gap, the dipole moment has an opposite effect for the pure CdS rod and the CdSe/CdS core/shell rod. For the pure CdS rod, the dipole moment reduces its band gap. In our system, it cancels out the stronger quantum confinement effect due to the reduction of the nanorod diameter. As a result, for the pure CdS rod, the Cd+S termination and the Cd termination have similar band gaps. However, in the CdSe/CdS core/shell nanorod, the dipole moment increases the band gap because the electron and hole localizations are determined by the band alignment effect, not the dipole moment. As a result, the dipole moment and the quantum confinement work together to increase the band gap in the CdSe/CdS core/shell and Cd+S termination case. All of these show very rich interplays between the different effects. They can be used as designing knobs for different nanostructure applications.

METHODS

The atomic structures of the system are relaxed using the valence force field model (VFF).[17] The ball-and-stick microscopic mechanical model is accurate for describing the elastic relaxations. For the VFF parameters, we have used the experimental bulk lattice constants and elastic coefficients. After the atomic positions are relaxed, the strain of atoms is calculated, and results of the hydrostatic strain are shown in Figure 2 for one CdSe/CdS core/shell nanorod.

To solve the electronic structure, we used the charge patching method[24] to construct the nanocrystal electron charge density from a set of bulk and surface charge motifs. These motifs are

generated from small prototype system calculations, under local density approximation of the density functional theory using a planewave pseudopotential method with a 35 Ry planewave energy cutoff. The charge motifs also include the derivative motifs describing the charge density changes due to the change of bond length and bond angle. After the electron charge density of the nanorod has been constructed, the band edge energies and wave functions are calculated by the folded-spectrum method (FSM).[25] To correct the LDA band gap error and to yield the correct effective masses, we have modified the nonlocal parts of the pseudopotentials in the FSM calculation.[20] This LDA+C (correction) approach has been successfully applied to quantum dot and rod nanocrystals[20,26] and spherical core/shell nanocrystals.[27] Spin-orbit couplings are included in the FSM calculations.

Acknowledgment. Y.L. is funded by the National Science Foundation of China under Contract No. 20873009. L.W.W. is supported by the U.S. Department of Energy, BES/SC under Contract No. DE-AC02-05CH11231. This research used the resources of the National Energy Research Scientific Computing Center (NERSC).

REFERENCES AND NOTES

1. Whang, D. M.; Song, J.; Mu, Y.; Lieber, C.; Whang, M.; D.; Jin, S.; Wu, Y.; Lieber, M. C. Large-Scale Hierarchical Organization of Nanowire Arrays for Integrated Nanosystems. *Nano Lett.* **2003**, *3*, 1255–1259.
2. Robinson, R. D.; Sadtler, B.; Demchenko, D. O.; Erdonmez, C. K.; Wang, L. W.; Alivisatos, A. P. Spontaneous Superlattice Formation in Nanorods through Partial Cation Exchange. *Science* **2007**, *317*, 355–358.
3. Talapin, D. V.; Koeppe, R.; Gotzinger, S.; Komowski, A.; Lupton, J. M.; Rogach, A. L.; Benson, O.; Feldmann, J.; Weller, H. Highly Emissive Colloidal CdSe/CdS Heterostructures of Mixed Dimensionality. *Nano Lett.* **2003**, *3*, 1677–1681.
4. Carbone, L.; Nobile, C.; Giorgi, M. D.; Sala, F. D.; Morello, G.; Pompa, P.; Hytch, M.; Snoeck, E.; Fiore, A.; Franchini, I. R.; *et al.* Synthesis and Micrometer-Scale Assembly of Colloidal CdSe/CdS Nanorods Prepared by a Seeded Growth Approach. *Nano Lett.* **2007**, *7*, 2942–2950.
5. Talapin, D. V.; Nelson, J. H.; Shevchenko, E. V.; Aloni, S.; Sadtler, B.; Alivisatos, A. P. Seeded Growth of Highly Luminescent CdSe/CdS Nanoheterostructures with Rod and Tetrapod Morphologies. *Nano Lett.* **2007**, *7*, 2951–2959.
6. Fiore, A.; Mastria, R.; Grazia-Lupo, M.; Lanzani, G.; Giannini, C.; Carlino, E.; Morello, G.; Giorgi, M. D.; Li, Y.; Cingolani, R.; *et al.* Tetrapod-Shaped Colloidal Nanocrystals of II−VI Semiconductors Prepared by Seeded Growth. *J. Am. Chem. Soc.* **2009**, *131*, 2274–2282.
7. Reiss, P.; Protiere, M.; Li, L. Core/Shell Semiconductor Nanocrystals. *Small* **2009**, *5*, 154–168.
8. Menagen, G.; Mocatta, D.; Salant, A.; Popov, I.; Dorfs, D.; Banin, U. Selective Gold Growth on CdSe Seeded CdS Nanorods. *Chem. Mater.* **2008**, *20*, 6900–6902.
9. Hewa-Kasakarage, N. N.; Kirsanova, M.; Nemchinov, A.; Schmall, N.; El-Khoury, P. Z.; Tarnovsky, A.; Zamkov, N. M. Radiative Recombination of Spatially Extended Excitons in (ZnSe/CdS)/CdS Heterostructured Nanorods. *J. Am. Chem. Soc.* **2009**, *131*, 1328–1334.
10. Steiner, D.; Dorfs, D.; Banin, U.; Sala, F. D.; Manna, L.; Millo, O. Determination of Band Offsets in Heterostructured Colloidal Nanorods Using Scanning Tunneling Spectroscopy. *Nano Lett.* **2008**, *8*, 2954–2958.
11. Lupo, M. G.; Sala, F. D.; Carbone, L.; Rossi, M. Z.; Fiore, A.; Loer, L.; Polli, D.; Cingolani, R.; Manna, L.; Lanzani, G. Ultrafast Electron−Hole Dynamics in Core/Shell CdSe/CdS Dot/Rod Nanocrystals. *Nano Lett.* **2008**, *8*, 4582–4587.
12. Morello, G.; Sala, F. D.; Carbone, L.; Manna, L.; Maruccio, G.; Cingolani, R.; Giorgi, M. D. Intrinsic Optical Nonlinearity in Colloidal Seeded Grown CdSe/CdS Nanostructures: Photoinduced Screening of the Internal Electric Field. *Phys. Rev. B* **2008**, *78*, 195313-1–195313-8.
13. Pokrant, S.; Whaley, K. B. Tight-Binding Studies of Surface Effects on Electronic Structure of CdSe Nanocrystals: The Role of Organic Ligands, Surface Reconstruction, and Inorganic Capping Shells. *Eur. Phys. J. D* **1999**, *6*, 255–267.
14. Manna, L.; Wang, L. W.; Cingolani, R.; Alivisatos, A. P. First-Principles Modeling of Unpassivated and Surfactant-Passivated Bulk Facets of Wurtzite CdSe: A Model System for Studying the Anisotropic Growth of CdSe Nanocrystals. *J. Phys. Chem. B* **2005**, *109*, 6183–6192.
15. Muller, J.; Lupton, J. M.; Lagoudakis, P. G.; Schindler, F.; Koeppe, R.; Rogach, A. L.; Feldnamm, J. Wave Function Engineering in Elongated Semiconductor Nanocrystals with Heterogeneous Carrier Confinement. *Nano Lett.* **2005**, *5*, 2044–2049.
16. Huang, X.; Lindgren, E.; Chelikowsky, J. R. Surface Passivation Method for Semiconductor Nanostructures. *Phys. Rev. B* **2005**, *71*, 165328-1–165328-6.
17. Pryor, C.; Kim, J.; Wang, L. W.; Williamson, A. J.; Zunger, A. Comparison of Two Methods for Describing the Strain Profiles in Quantum Qots. *J. Appl. Phys.* **1998**, *83*, 2548–2554.
18. Cardona, M.; Weinstein, M.; Wolff, G. A. Ultraviolet Reflection Spectrum of Cubic CdS. *Phys. Rev.* **1965**, *140*, A633–A637.
19. Dai, Q.; Song, Y.; Li, D.; Chen, H.; Kan, S.; Zou, B.; Wang, Y.; Deng, Y.; Hou, Y.; Yu, S.; *et al.* Temperature Dependence of Band Gap in CdSe Nanocrystals. *Chem. Phys. Lett.* **2007**, *439*, 65–68.
20. Li, J.; Wang, L. W. Band-Structure-Corrected Local Density Approximation Study of Semiconductor Quantum Dots and Wires. *Phys. Rev. B* **2005**, *72*, 125325-1–125325-15.
21. Sitt, A.; Sala, F. D.; Menagen, G.; Banin, U. Multiexciton Engineering in Seeded core/shell Nanorods: Transfer from Type-I to Quasi-type-II regimes. *Nano Lett* **2009**, *9*, 3470–3476.
22. Langbein, W.; Hetterich, M.; Klingshirn, C. Many-Body Effects and Carrier Dynamics in CdSe/CdS Stark Superlattices. *Phys. Rev. B* **1995**, *51*, 9922–9929.
23. Bradley, I. V.; Creasey, J. P.; O'Donnell, K. P.; Wright, P. J.; Cockayne, B. CdS−CdSe and CdS−ZnSe Intrinsic Stark Superlattices. *J. Cryst. Growth* **1996**, *159*, 551–554.
24. Wang, L. W. Charge-Density Patching Method for Unconventional Semiconductor Binary Systems. *Phys. Rev. Lett.* **2002**, *88*, 256402-1–256402-4.
25. Wang, L. W.; Zunger, A. Solving Schrödinger's Equation Around a Desired Energy: Application to Silicon Quantum Dots. *J. Chem. Phys.* **1994**, *100*, 2394–2397.
26. Li, J.; Wang, L. W. First-Principles Thousand-Atom Quantum Dot Calculations. *Phys. Rev. B* **2004**, *69*, 153302-1–153302-4.
27. Schrier, J.; Wang, L. W. Electronic Structure of Nanocrystal Quantum Dot Quantum Wells. *Phys. Rev. B* **2006**, *73*, 245332-1–245332-6.